International Journal on Magnetic Particle Imaging
Vol 5, No 1-2, Article ID 1906001, 7 Pages

Infinite Science Publishing

Research Article

Remote Detection of Magnetic Signals with a Compact Atomic Magnetometer Module Towards Human MRI–MPI Hybrid Systems

Takenori Oida[a,*] · Kentaro Kato[a] · Yosuke Ito[a] · Tetsuo Kobayashi[a]

[a]Department of Electrical Engineering, Graduate School of Engineering, Kyoto University, Japan
*Corresponding author, email: oida@kuee.kyoto-u.ac.jp

Received 13 November 2018; Accepted 06 May 2019; Published online 18 June 2019

Abstract

This study demonstrates the possibility of remotely detecting magnetic fields generated from superparamagnetic iron oxide nanoparticles using a compact optically pumped atomic magnetometer (OPAM) module with a flux transformer (FT) during the development of magnetic resonance imaging–magnetic particle imaging (MRI–MPI) hybrid systems. Results of previous studies particularly demonstrated odd harmonics of the magnetic nanoparticle (MNP) signals. In addition, studies have demonstrated that the magnitude of odd harmonics was proportional to the quantity of magnetic nanoparticles, and the minimum MNP quantity can possibly be estimated from signal measurements. In conclusion, experimental results suggested that MNP signals from the Resovist solution with Fe of 0.01 μmol could be detected using a compact OPAM module with FT as an ultra-low field–magnetic resonance imaging detector.

I. Introduction

Magnetic particle imaging (MPI) can determine high-speed hemodynamic imaging [1–3] employed as a new method to measure biological functions. In MPI, an induction coil detects magnetic signals generated via the magnetization of magnetic nanoparticles (MNPs), characterized by nonlinear magnetization. This results in high-speed and high spatial resolution imaging. However, considering the specific absorption rate and time-varying magnetic field (dB/dt), which are limited to minimize risks in human health, magnetic signals should be measured in a low-frequency range to obtain *in vivo* MPI measurements.

In recent years, optically pumped atomic magnetometers (OPAMs) have been widely known because of the affordability and availability of technologies required for their fabrication. OPAMs are performed by detecting the electron spin precession in alkali-metal atoms contained in a glass cell [4, 5]. At the beginning of this century, OPAMs operating in spin exchange relaxation free conditions have reached sensitivities comparable to or even exceeding those of superconducting quantum interference devices (SQUIDs) [6–8]. The most sensitive OPAM has a sensitivity in the subfemtotesla per root square hertz range [8].

Since OPAMs are intrinsically advantageous because it does not require cryogenic cooling, they are currently expected to exceed SQUIDs, and their use for biomagnetic field measurements [9–13] has been effectively demonstrated. For instance, OPAMs have been used to perform magnetoencephalography (MEG) in neuroscience and fetal magnetocardiography, high-precision fundamental physical experiments, inertia-based mea-

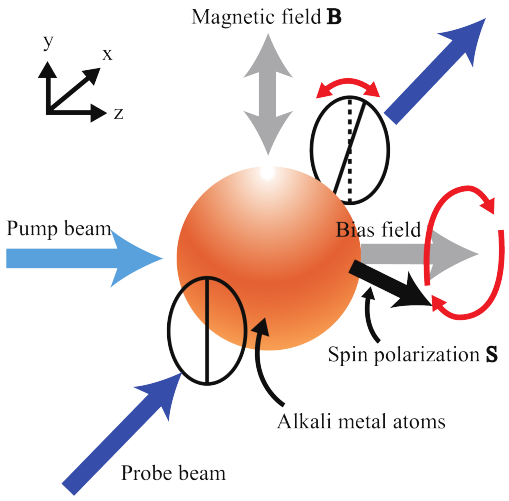

Figure 1: The OPAM principle. Alkali-metal electron spins are polarized using a circularly polarized pump beam. In the presence of the bias magnetic field parallel to the pump beam, electron spins evolve around the bias magnetic field when the alternating or rotating magnetic field is applied orthogonally. Then, the x component of electron spins are measured based on the magneto-optical effect of a linearly polarized probe beam.

surements, and magnetic resonance imaging (MRI) [14, 15].

In addition, OPAMs can be fabricated in sizes smaller than those of SQUIDs; therefore, they can be placed closer to the field source, which results in increased signal strength. This allows more freedom for sensor placement, a feature very welcome in the MEG field.

OPAMs used as a detector instead of an induction coil are expected to be capable of operating MPI scanners at a relatively low excitation or driving frequency because of their tunable sensitive frequency. This is an important advantage in fabricating clinical human-sized MPI scanners.

This study aimed to measure MNP signals from superparamagnetic iron oxide (SPIO) magnetic particles in order to establish clinical MRI–MPI hybrid systems with OPAMs in the low-frequency range and to demonstrate their feasibility.

II. Methods

II.I. OPAM Principles

This study used an OPAM with a pump-probe arrangement consisting of two laser beams [4]. A circularly polarized pump beam and a linearly polarized probe beam crossed orthogonally at the center of the glass cell including vaporized alkali-metal atoms, as shown in Figure 1. The wavelength of a pump beam was tuned to D1 line of alkali-metal atoms. Their electron spins were polarized using and following the direction of the pump beam.

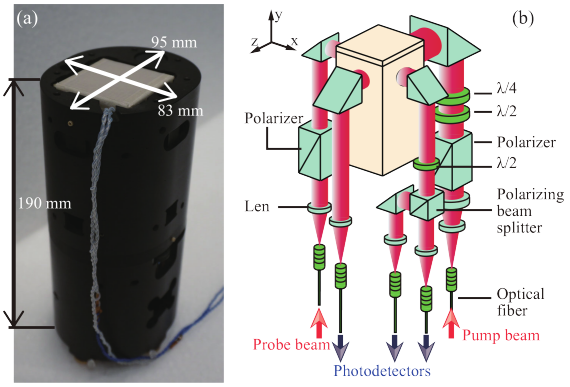

Figure 2: Appearance of a compact OPAM module with potassium atoms [13] (a). Optical component arrangements (b).

When applying a magnetic field **B** perpendicular to the pump and probe beams, electron spins evolved, and the polarization plane of the linearly polarized probe beam is rotated using electron spin components along the probe beam. When the rotation angle is proportional to the spin polarization component along the probe beam, the magnetic field strength can be measured. The evolution of electron spin polarization **S** can be described using the Bloch equations [16, 17].

II.II. OPAM module

Our previous study has focused on the development of an ultra-high-sensitivity OPAM [16–19]. Recently, a compact and portable module of potassium OPAM was successfully fabricated with a pump-probe arrangement as the sensing atom (Figure 2) [13]. The OPAM module has an elliptic cylindrical shape. The top and bottom areas are approximately 64 cm^2 with the height of 19 cm. The sensor region at which the pump beam intersects with the probe beam is located 2.2 cm from the top surface of the OPAM module, as shown in Figure 2(a). The OPAM module itself used two laser beams known as the pump and probe, placed perpendicular to each other. The probe laser is linearly polarized, whereas the pump laser is circularly polarized. Because the noise spectrum density of the OPAM reached 21 $fT_{rms}/Hz^{1/2}$ at 10 Hz, human MEGs were measured [13].

The sensor head cell contained potassium with He and N_2 as buffer gases in a 10:1 ratio to reduce diffusion of potassium atoms to cell walls and for quenching. The sensor head was placed in a thermally insulated, cubic, Pyrex glass cell with a side length of 20 mm, and heated to 180 °C using a resistive heating element driven by a power amplifier at 100 kHz. A more detailed discussion on the module's design is presented in our previous paper [13].

The OPAM module was also used to detect NMR signals, and MRI was performed with an OPAM module at an ultra-low field (ULF), i.e., below 1 mT [20]. As

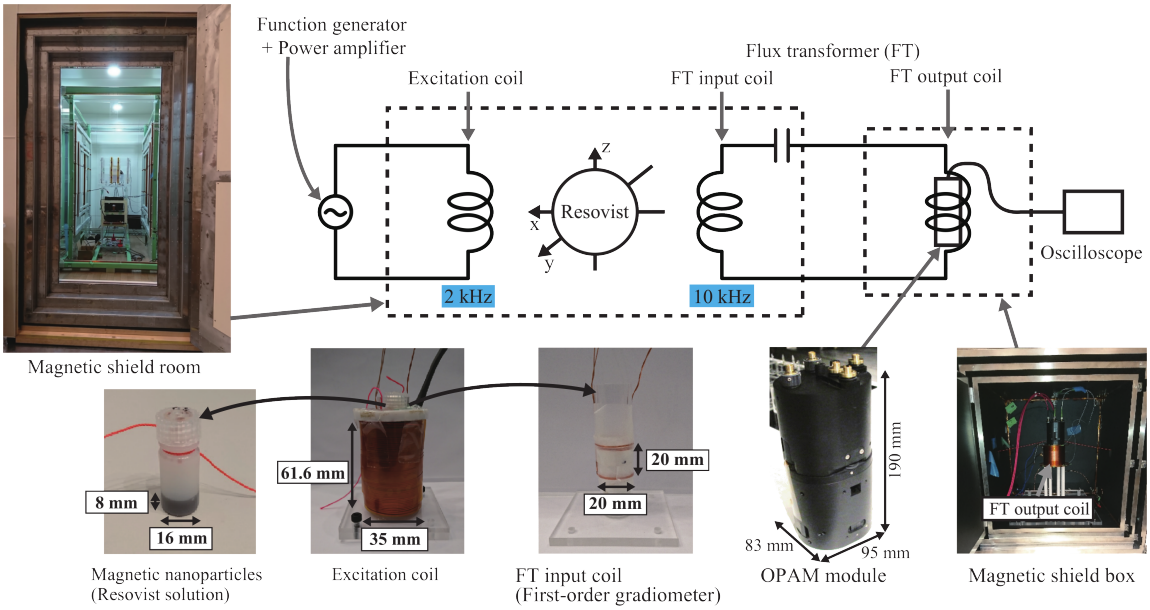

Figure 3: Experimental set-up. Excitation fields were applied in three-layered magnetic shield room. MNP signals generated from Resovist solutions were transferred through a flux transformer (FT) to another magnetic shield box. In the shield box, magnetic signals caused by MNPs were detected using an OPAM module through the FT.

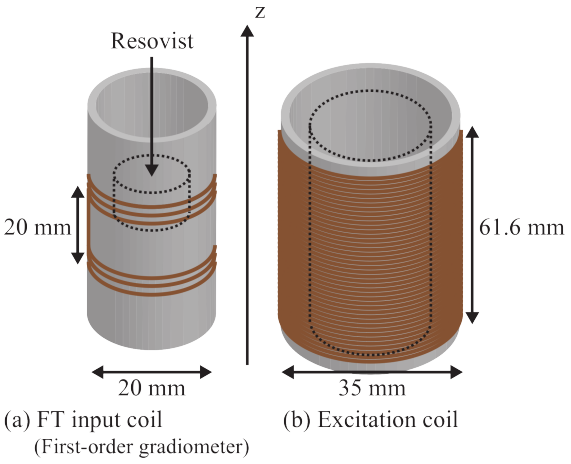

Figure 4: Detail schematics of the first-order gradiometer type input coil of flax transformer (a) and excitation coil (b).

OPAMs were successfully used as receiving sensors for pre-polarized ULF–MRI systems because of their high sensitivity in low-frequency ranges, they are also expected to yield promising results when used with MPI scanners [21].

II.III. Experimental Set-up

Figure 3 shows the experimental set-up. Magnetic nanoparticles, an FT input coil, and an excitation coil were placed in a three-layered magnetically shielded room (Figure 3 top left), whereas the OPAM module was placed in another three-layered magnetically shielded box (Figure 3 bottom right). In the shielded box containing the OPAM module, three pairs of orthogonal coils were built to compensate the residual background field and apply a bias field along the pump beam. Its sensitivity was 10-100 fT/Hz$^{1/2}$ at frequencies below several kHz.

During the experiments, excitation fields oscillating sinusoidally were applied to magnetic nanoparticles. The magnetic nanoparticle solution containing ferucarbotran known as Resovist® (Fujifilm RI Pharma Co.) was placed in a 16 mm-diameter container (Figure 3 bottom left), and the height of the Resovist solution in the container was then adjusted to 8 mm.

As shown in the bottom right of Figure 3, the FT output coil was placed around the OPAM module, which consisted of 94 turns of the FT output coil. Figure 4(a) shows the configuration of the FT input coil. The first-order gradiometer was produced as the FT input coil to reduce the induction voltage from the excitation field as much as possible. The coil was made from a copper wire measuring 0.5 mm in diameter and configured with three turns on the upper and three on the lower portions of the cylinder with a baseline (distance between the centers of upper and lower coils) of 20 mm. The resonance frequency of the FT circuit was tuned to 10 kHz to measure the harmonics at 2 kHz.

A 1 mm × 1 mm square wire was used to configure an excitation coil consisting of four layers: 48, 49, 52, and 52 turns from the inside. The inner diameter was 28.6 mm, and the outer diameter was 35 mm, with the height of 61.6 mm (Figure 4(b)). In addition, sinusoidal

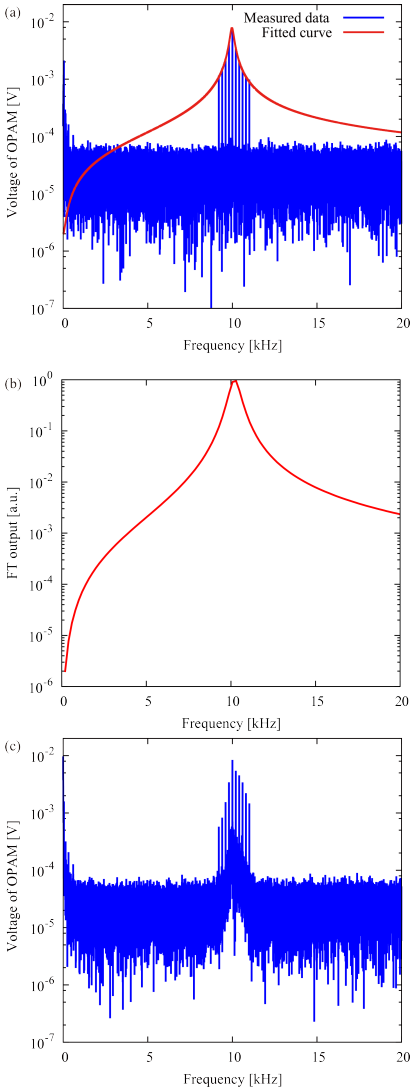

Figure 5: Frequency responses of OPAM (a) and FT (b), and the MNP signal detector with OPAM and FT (c).

currents were supplied to the excitation coil using a function generator and an amplifier. In the experiment, the OPAM module was tuned to 10 kHz by applying the bias magnetic field along the direction of the pump beam.

III. Results

First, to evaluate the frequency response characteristics of the detector with an OPAM and an FT, reference magnetic fields were applied to the OPAM module or the FT input coil. To measure the frequency of OPAM responses, reference fields consisted of ten sinusoidal fields with 7.1 pT_{rms} in amplitude and frequencies from 9.2 to 11.0 kHz with increment of 0.2 kHz, as generated by a Helmholtz coil. Figure 5(a) shows the frequency OPAM module responses. Figure 5 also demonstrates that frequency responses of each reference field with 9.2,

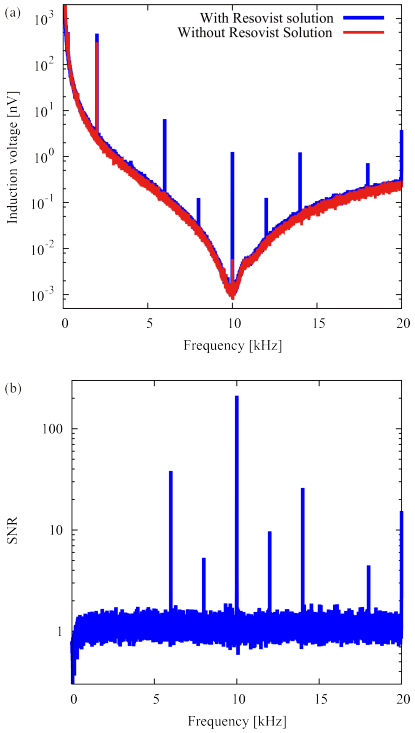

Figure 6: Frequency characteristics of signal-to-noise ratio (SNR). (a) Induction voltages of FT input coil with (red line) and without (blue line) Resovist solution. (b) SNR calculated from induction voltages.

9.4, ..., 11.0 kHz were fitted to the expected responses, which were calculated using the Bloch equations of the electron spins in the OPAM module [22]. These results indicated that the resonant frequency of OPAM was well tuned to approximately 10 kHz with the sensitivity of 29.2 $fT_{rms}/Hz^{1/2}$ and its bandwidth was approximately 230 Hz. In addition, Figure 5(b) shows the normalized frequency responses in FT. The FT was tuned to approximately 10 kHz, with a bandwidth of approximately 720 Hz.

To obtain the frequency response characteristics of the detector with an OPAM and FT, reference magnetic fields were applied to the FT input coil. The reference magnetic fields were generated using a two-turn loop coil with a diameter of 23 mm on the upper portion of the FT input coil. The reference magnetic fields consisted of ten sinusoidal fields with an amplitude of 800 pT_{rms}. Figure 5(c) shows the frequency responses of the detector with the OPAM and FT. These results showed that the detector was also tuned to approximately 10 kHz, whereas the noise of approximately 10 kHz increased as compared with that of OPAM module only.

Next, to compare the MNP signal and noise, induction voltages of the FT input coil were obtained using the OPAM with and without the Resovist solution with 4 µmol of Fe. In these measurements, the excitation field with an amplitude of 4.56 mT and frequency of 2 kHz

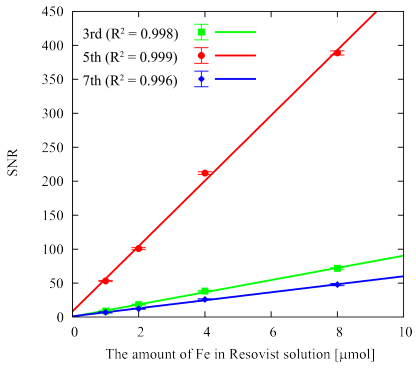

Figure 7: SNRs as a function of the amount of Fe. The means (marker) and SDs (error bars) of SNRs caused by the Resovist solutions with Fe of 1, 2, 4, and 8 μmol.

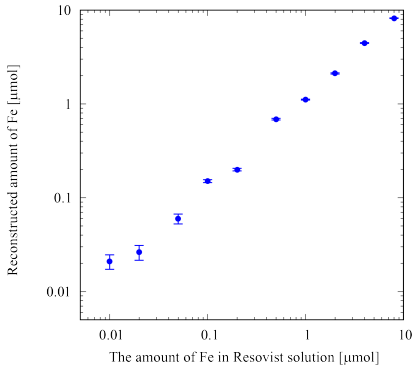

Figure 8: Means (marker) and SDs (error bars) of the reconstructed amount of Fe in each Resovist solution estimated by the system function.

were applied to generate MNP signals. In addition, induction voltages were recorded for 1 s and analyzed using the fast Fourier transformation to obtain the harmonics. Frequency responses of induction voltages with and without the Resovist solution are shown in Figure 6(a), where the blue line is an example of a frequency response to the induction voltage generated from the MNP magnetization in the Resovist solution. In addition, the red line in Figure 6(a) is an example of noises caused by interference effects in the excitation field on the FT input coil. When comparing these two induction voltages, increases in voltages at the 3rd, 5th, and 7th harmonics (6, 10, and 14 kHz) of the excitation frequency were caused by the Resovist solution, known as MNP signals. In addition, the signal-to-noise ratios (SNRs) where the noise is primarily caused by interference in the excitation fields to the FT input coil are shown in Figure 6(b), demonstrating the 5th harmonic of the excitation frequency was 5 times larger than the 3rd or 7th harmonics.

Conversely, SNR means and standard deviations (SDs) caused by the Resovist solutions with Fe of 1, 2, 4, and 8 μmol are shown in Figure 7, which demonstrates that SDs of SNR in the 3rd, 5th and 7th harmonics were

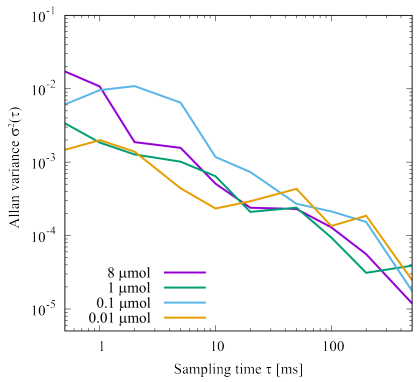

Figure 9: The Allan variances of the reconstructed amount of Fe with 8, 1, 0.1 and 0.01 μmol based on the sampling time.

obtained by dividing the SDs of the amplitude in each harmonic of MNP signals according to the noise level, that is, the mean amplitude in each harmonic measured without Resovist. Additionally, to confirm the linearity of MNP signals with the amount of nanoparticles, linear regression analyses of SNRs were performed based on the amount of Fe in the Resovist solution. Figure 7 indicates that SNR linearity with respect to the amount of nanoparticles is adequate.

In addition, the means and SDs of the reconstructed amount of Fe in each Resovist solution are shown in Figure 8. In these measurements, MNP signals were generated using an excitation field with 4.56 mT amplitude and 2 kHz frequency. The 1 s MNP signals were then recorded and analyzed using the system function [3]. In this analysis, the system function (system matrix) is estimated based on the frequency responses of 30-averaged MNP signal with 8 μmol Fe using the system function method proposed by Kosch et al. [23]. Figure 8 shows that the amounts of Fe could be reconstructed using the system function. However, although the amount of Fe in the Resovist solution can be reconstructed based on MNP signals of 0.01 μmol obtained using the detector with an OPAM and FT, the reconstructed amount with Fe of 0.01 μmol was approximately twice of the prepared solution.

Finally, to rapidly scan MNP signals, Allan variances [24] in the reconstructed amount of Fe estimated using the system function are shown in Figure 9. In the analyses, the MNP signals used were the same as in Figure 8, and the sampling time τ from 0.5 ms, that is, the cycle of the excitation field to 500 ms was evaluated. The results indicate that variances become smaller as the time of measurement are prolonged. Since the variance is large when the sampling time is <10 ms, the sufficient reconstruction accuracy may not be obtained.

IV. Discussion

Based on reference field measurements, an MNP signal detector with OPAM module and FT as the magnetic sensor with a relatively high sensitivity of approximately 10 kHz was tuned to the resonant frequency of the detector with a narrow bandwidth of approximately 230 Hz in the OPAM and approximately 720 Hz in the FT. Since these bandwidths are narrow, high-order harmonics of 2 kHz cannot be measured. MPI measurements with OPAM and FT yields similar results on the narrowband MPI, as reported by Goodwill et al. [25].

Conversely, Figures 6 and 7 show that when MNP signals were greater than the noises and interferences caused by the excitation field with 2 kHz, ratios of the MNP signal to the interference or noise were linearly correlated with the amount of MNPs. MNP signals could also be detected with higher SNRs especially in the 5th harmonic of the excitation field, to which the OPAM and the FT were tuned. The feasibility of MRI–MPI hybrid systems with OPAM and FT can possibly be demonstrated because the detector could be used for ULF–MRI measurements. However, interference effects from the excitation field on the input coil of FT were greater than the noise level of the detector with an OPAM and an FT in the 5th harmonic.

Therefore, the interference of the excitation field should be suppressed further to reduce the effects on the FT input coil in order to obtain MNP signals from a smaller amount of nanoparticles. However, measurements were carried out using a small input coil that is appropriate to the sample in this study. Therefore, in case of a large input coil in humans, a detector with an OPAM and an FT is expected to be performed similarly as in this experiment to prevent a series input coil resistance.

In addition, although the linearity between the SNR and amount of nanoparticles becomes low, MNP signals generated by nanoparticles of 0.01 µmol could be detected using the OPAM and the FT in the sampling time of 1 s. However, to detect MNP signals caused by MNPs of <0.01 µmol, the interference from the excitation field should be reduced because the detector's sensitivity in measuring MNP signals was limited by the interference.

However, Figure 9 shows a tradeoff between the SNR and the sampling time during the MNP signal analysis. Therefore, the SNR of an OPAM + FT should be improved for rapid MPI measurement with an OPAM.

V. Conclusion

In this study, MNP signals of <10 kHz generated from the SPIO magnetization were measured using a compact OPAM module and an FT with a first-order gradiometer input coil as the detector in order to determine the feasibility of using MRI–MPI hybrid systems in humans with an OPAM operated in the low-frequency range.

According to MNP measurement results, MNP signals from the Resovist solution with Fe of 0.01 µmol could be remotely measured using our detector, generated based on the excitation field of 4.56 mT amplitude and 2 kHz frequency.

In addition, the SNR of MNP signals was obtained using short sampling times to reduce the scan time of harmonic-space imaging with an OPAM. Based on these results, MNP signals generated using the Resovist solution with Fe of 0.1 µmol could be obtained by using the same detector with an OPAM + FT in ULF–MRI, although SNRs obtained using a sampling time of 10 ms were reduced to half of those in 1 s. These results suggest that a compact OPAM module + FT is a feasible detector technology for human MRI–MPI hybrid systems operated in a low-frequency range.

Acknowledgements

This work was partially supported by the Grant-in-Aid for Research (15H01813, JP17K20104) from the Ministry of Education, Culture, Sports, Science and Technology (MEXT), Japan, and the Grant for Research from Nakatani Foundation for Advancement of Measuring Technology in Biomedical Engineering.

References

[1] B. Gleich and J. Weizenecker. Tomographic imaging using the nonlinear response of magnetic particles. *Nature*, 435(7046):1214–1217, 2005, doi:10.1038/nature03808.

[2] P. W. Goodwill and S. M. Conolly. The X-Space Formulation of the Magnetic Particle Imaging Process: 1-D Signal, Resolution, Bandwidth, SNR, SAR, and Magnetostimulation. *IEEE Transactions on Medical Imaging*, 29(11):1851–1859, 2010, doi:10.1109/TMI.2010.2052284.

[3] T. Knopp and T. M. Buzug, Magnetic Particle Imaging: An Introduction to Imaging Principles and Scanner Instrumentation. Berlin, Heidelberg: Springer Berlin Heidelberg, 2012, doi:10.1007/978-3-642-04199-0.

[4] D. Budker and M. Romalis. Optical magnetometry. *Nature Physics*, 3(4):227–234, 2007, doi:10.1038/nphys566.

[5] D. Budker and D. F. Jackson Kimball, Eds., Optical Magnetometry. Cambridge: Cambridge University Press, 2013, doi:10.1017/CBO9780511846380.

[6] J. C. Allred, R. N. Lyman, T. W. Kornack, and M. V. Romalis. High-Sensitivity Atomic Magnetometer Unaffected by Spin-Exchange Relaxation. *Physical Review Letters*, 89(13):130801, 2002, doi:10.1103/PhysRevLett.89.130801.

[7] I. K. Kominis, T. W. Kornack, J. C. Allred, and M. V. Romalis. A subfemtotesla multichannel atomic magnetometer. *Nature*, 422(6932):596–599, 2003, doi:10.1038/nature01484.

[8] H. B. Dang, A. C. Maloof, and M. V. Romalis. Ultrahigh sensitivity magnetic field and magnetization measurements with an atomic magnetometer. *Applied Physics Letters*, 97(15):151110, 2010, doi:10.1063/1.3491215.

[9] H. Xia, A. Ben-Amar Baranga, D. Hoffman, and M. V. Romalis. Magnetoencephalography with an atomic magnetometer. *Applied Physics Letters*, 89(21):211104, 2006, doi:10.1063/1.2392722.

[10] K. Kamada, Y. Ito, and T. Kobayashi. Human MCG measurements with a high-sensitivity potassium atomic magnetometer. *Physiological Measurement*, 33(6):1063–1071, 2012, doi:10.1088/0967-3334/33/6/1063.

[11] T. H. Sander, J. Preusser, R. Mhaskar, J. Kitching, L. Trahms, and S. Knappe. Magnetoencephalography with a chip-scale atomic magnetometer. *Biomedical Optics Express*, 3(5):981, 2012, doi:10.1364/BOE.3.000981.

[12] V. K. Shah and R. T. Wakai. A compact, high performance atomic magnetometer for biomedical applications. *Physics in Medicine and Biology*, 58(22):8153–8161, 2013, doi:10.1088/0031-9155/58/22/8153.

[13] K. Kamada, D. Sato, Y. Ito, H. Natsukawa, K. Okano, N. Mizutani, and T. Kobayashi. Human magnetoencephalogram measurements using newly developed compact module of high-sensitivity atomic magnetometer. *Japanese Journal of Applied Physics*, 54(2):026601, 2015, doi:10.7567/JJAP.54.026601.

[14] I. Savukov, V. Zotev, P. Volegov, M. Espy, A. Matlashov, J. Gomez, and R. Kraus. MRI with an atomic magnetometer suitable for practical imaging applications. *Journal of Magnetic Resonance*, 199(2):188–191, 2009, doi:10.1016/j.jmr.2009.04.012.

[15] I. Savukov and T. Karaulanov. Anatomical MRI with an atomic magnetometer. *Journal of Magnetic Resonance*, 231:39–45, 2013, doi:10.1016/j.jmr.2013.02.020.

[16] K. Kamada, S. Taue, and T. Kobayashi. Optimization of Bandwidth and Signal Responses of Optically Pumped Atomic Magnetometers for Biomagnetic Applications. *Japanese Journal of Applied Physics*, 50(5):056602, 2011, doi:10.1143/JJAP.50.056602.

[17] S. Taue, Y. Sugihara, T. Kobayashi, K. Ishikawa, and K. Kamada. Magnetic Field Mapping and Biaxial Vector Operation for Biomagnetic Applications Using High-Sensitivity Optically Pumped Atomic Magnetometers. *Japanese Journal of Applied Physics*, 50:116604, 2011, doi:10.1143/JJAP.50.116604.

[18] Y. Ito, H. Ohnishi, K. Kamada, and T. Kobayashi. Development of an optically pumped atomic magnetometer using a K-Rb hybrid cell and its application to magnetocardiography. *AIP Advances*, 2(3):032127, 2012, doi:10.1063/1.4742847.

[19] K. Kamada, Y. Ito, S. Ichihara, N. Mizutani, and T. Kobayashi. Noise reduction and signal-to-noise ratio improvement of atomic magnetometers with optical gradiometer configurations. *Optics Express*, 23(5):6976, 2015, doi:10.1364/OE.23.006976.

[20] I. Hilschenz, Y. Ito, H. Natsukawa, T. Oida, T. Yamamoto, and T. Kobayashi. Remote detected Low-Field MRI using an optically pumped atomic magnetometer combined with a liquid cooled pre-polarization coil. *Journal of Magnetic Resonance*, 274:89–94, 2017, doi:10.1016/j.jmr.2016.11.006.

[21] S. Colombo, V. N. Lebedev, A. Tonyushkin, Z. D. Grujic, V. Dolgovskiy, and A. Weis. Towards a mechanical MPI scanner based on atomic magnetometry. *International Journal on Magnetic Particle Imaging*, 3(1), 2017, doi:10.18416/IJMPI.2017.1703006.

[22] T. Oida, Y. Ito, K. Kamada, and T. Kobayashi. Detecting rotating magnetic fields using optically pumped atomic magnetometers for measuring ultra-low-field magnetic resonance signals. *Journal of Magnetic Resonance*, 217:6–9, 2012, doi:10.1016/j.jmr.2012.01.015.

[23] O. Kosch, U. Heinen, L. Trahms, and F. Wiekhorst. Preparing system functions for quantitative MPI. *International Journal on Magnetic Particle Imaging*, 3(2), 2017, doi:10.18416/IJMPI.2017.1706002.

[24] D. Allan. Statistics of atomic frequency standards. *Proceedings of the IEEE*, 54(2):221–230, 1966, doi:10.1109/PROC.1966.4634.

[25] P. Goodwill, G. Scott, P. Stang, and S. Conolly. Narrowband Magnetic Particle Imaging. *IEEE Transactions on Medical Imaging*, 28(8):1231–1237, 2009, doi:10.1109/TMI.2009.2013849.

